Kurdish Studies
September, 2024
Volume: 12, No: 4, pp 1907-1917
ISSN: 2051-4883 (Print) | ISSN 2051-4891 (Online)
www.KurdishStudies.net

DOI: 10.53555/ks.v12i4.3734

Traveling Wave Solution and Stability Analysis of Non-Newtonian Unsteady Fluid Flow

Muhammad Hussan[1]*, Ashir Ashfaq[2]*, Muhammad Irshad[3], Atifa Latif[1]

[1]Department of Mathematics, Government College University Faisalabad, 38000, Faisalabad, Pakistan.
[2]Department of Mathematics, Punjab College University Campus, 38000, Faisalabad, Pakistan.
[3]Department of Mathematics, Ripha Internatonal University, Main Satyana Road, Faisalabad 38000, Pakistan.

***Corresponding author:** Muhammad Hussan, Ashir Ashfaq
**Email addresses:* m_hussan_mann@hotmail.com (Muhammad Hussan), ashirashfaq1234@gmail.com (Ashir Ashfaq)

Abstract
This paper concentrates on traveling wave approximation, phase plane, and stability analysis of non-Newtonian fluids. The analysis is extended for the dynamical system theory of the problem to understand the flow behavior. Higher-order nonlinear autonomous differential equations are studied. These equations characterize the trajectories of the particles. The phase plots are drawn to show the qualitative behavior of the fluid flow. Equilibrium points are calculated and bifurcation diagrams are drawn for the complete range of parameters. Equilibria plots depict a detailed discussion of various flow patterns developed for the complete range of flow variables contrary to the current which describes the topological structure at some particular value of the parameter. Also, compare our numerical solution to the HAM solution and get an exceptional result.

Keywords: Third grade fluid, Traveling wave, Dynamical theory, Stability analysis, Bifurcation theory

1. Introduction

The modeling of materials with dense molecular structures, such as geological materials, polymer solutions, slurries, hydrocarbon oils, blood, and paints, is part of the study of non-Newtonian fluids. These materials have viscoelastic properties, similar to liquids and solids. As a result, understanding the complicated behavior and features of non-Newtonian fluids has never been more essential. Non-Newtonian fluid flow issues have a wide range of technological applications in engineering and industry. In comparison, the non-Newtonian fluids are un-identical with Newtonian fluids. As a result, one cannot substitute the behavior of Newtonian fluid with that of non-Newtonian fluid in feasible uses also, to gain a comprehensive understanding and enhance usage in the various manufacturing processes it is crucial to analyze and understand the behavior of non-Newtonian fluids.

The class of Rivlin-Ericksen fluids of differential type [16] is a generally recognised model among non-Newtonian fluids. Rivlin-Ericksen fluids have received specific attention in order to characterise a variety of unusual non-Newtonian fluid properties such as rod climbing, shear thinning, shear thickening, and normal stress effects. A review of the literature reveals that substantial attention has been paid to the flow difficulties of a second grade fluid [7, 8, 20, 21]. A second grade fluid model is the simplest subclass of differential type fluids for which an analytic result may be realistically expected. The governing equations for a second grade fluid are linear in most flow features. Although a second grade fluid model for steady flows is used to forecast normal stress differences, if the shear viscosity is considered to be constant, it does not correlate to shear thinning or thickening. As a result, third grade fluid may well explain several studies. A third-grade fluid mathematical model provides a more accurate explanation of the behaviour of nonNewtonian fluids. A third grade fluid model is an additional attempt to investigate the flow characteristics of non-Newtonian fluids. As a result, in this work, a third-grade fluid model was explored. This model has been shown to incorporate non-Newtonian effects such as shear thinning and thickening, as well as normal stress. Fosdick and Rajagopal [9] performed a thorough thermodynamic analysis of third-grade fluid and demonstrated the constraint on the stress constitutive equation. They explored various stability properties of third grade fluids and discovered that they differ from Newtonian and second grade fluids. Furthermore, Refs [1, 3, 10, 11, 12, 14, 15, 18, 23] provide several important messages dealing with third-grade fluid flow difficulties.

The motivation of this work is to investigate further properties of Non-Newtonian fluid. We in this paper have adopted the traveling wave approximation and then apply the dynamical systems theory to do the qualitative analysis of the solution of the problem [6]. This approach is a great success in finding the behavior of the complex fluids and has been rarely adopted in the reported studies.

The motivation of this work is to investigate further properties of Non-Newtonian fluid by applying the theory of dynamical systems, traveling wave approximations, and bifurcation analysis on the problem taken from the literature [6]. The dynamical systems are a contemporary advancement to find the nature (qualitative) of the problem by studying the stability through the bifurcation diagrams [2, 4, 5, 13, 19, 22]. The stability of the solution is not only significant mathematically nevertheless it is necessary to figure out if the solution remains credible as the time becomes infinite. Also, the qualitative behavior of the problem is very responsive to the involved parameters and thus depends on these parameters essentially. These important

features are highlighted in this research. The discussion is accomplished by inspecting the equilibria of the system and illustrating the mathematical model. These points (stagnation/critical points/equilibrium points/fixed points) are steady-state solutions. The stagnation points will be discriminated according to their qualitative nature as nodes, centers, and foci by looking at the eigenvalues. Local behavior is studied by performing the linear stability analysis with a discernment that the global behavior can be inferred. The plotted sketches will depict the qualitative nature of the solution. The bifurcation diagrams against various parameters are plotted to predict the qualitative behavior.

Following is the layout of the current paper: In section 2, the mathematical formulation of the physical model is given. Section 3 deals with the traveling wave solution for the unsteady flow of a third-grade fluid model embedded in a porous medium. The dynamical system theory is applied to the reduced ordinary differential equation. The qualitative behavior of the calculated critical points is decided based on eigenvalues. The phase plots are drawn against various characterizing parameters. It is observed that a higher-order dynamical system may help to investigate the flow behavior adequately. In section 4, the Normal mode method [24] is applied to check the stability of the problem. In section 5, the bifurcation diagrams are drawn against various characterizing parameters which shows the validity of the solution as time goes to infinity. Section 6 shows the validation and numerical schematic of the problem. The conclusion is presented at the end.

2. Mathematical Formulation

A Cartesian coordinate system *OXY Z* is considered in which *y*-axis is in the vertical (upward) direction and *x*-axis is along the direction of the porous plate at $y = 0$. The porous half space $y > 0$ is occupied by the fluid. As the plate is infinite in the *XZ*-plane, all the involved quantities (physical) excluding pressure depend on *y*. Consider a velocity of the form

$$\mathbf{U} = \left[u_1(y,t), -W_0, 0\right], \tag{1}$$

where u_1 is the velocity of the fluid in x-direction and $W_0 < 0$ denotes injection or blowing velocity whereas $W_0 > 0$ represents suction velocity. Eq. (1) satisfies the law of conservation of mass for incompressible fluid, i.e.

$\nabla \cdot \mathbf{U} = 0$.

Unsteady motion by a porous medium is given by (2)

$$\rho \frac{d\mathbf{U}}{dt} = \nabla \cdot \mathbf{T} + \mathbf{r_1}, \tag{3}$$

$$\frac{d}{dt} = \frac{\partial}{\partial t} + (\mathbf{U} \cdot \nabla).$$

we know that

$$\frac{d}{dt} = \frac{\partial}{\partial t} + (\mathbf{U} \cdot \nabla).$$

Incorporating in Eq. (3) we get,

$$\rho\left(\frac{\partial}{\partial t} + (\mathbf{U} \cdot \nabla)\right)\mathbf{U} = \nabla \cdot \mathbf{T} + \mathbf{r_1},$$

$$\rho \frac{\partial \mathbf{U}}{\partial t} + \mathbf{U} \cdot \nabla)\mathbf{U} = \nabla \cdot \mathbf{T} + \mathbf{r_1},$$

$$\rho\left[\frac{\partial u_1}{\partial t} - W_0 \frac{\partial u_1}{\partial y}\right] = \nabla \cdot \mathbf{T} + \mathbf{r_1}. \tag{4}$$

Where ρ is the fluid density, $\frac{d}{dt}$ is the material time derivative, **T** is the Cauchy stress tensor and **r** is the Darcy's resistance due to porous media.

The constitutive equation for a third-grade fluid is given in the literature

$$\mathbf{T} = -p\mathbf{I} + \mu\mathbf{A}_1 + \alpha_1\mathbf{A}_2 + \alpha_2\mathbf{A}_1^2 + \beta_3\left(trace\mathbf{A}_1^2\right)\mathbf{A}_1. \tag{5}$$

From above equation, p defines pressure, **I** denotes the identity tensor, μ reads as the dynamic viscosity, the material constants are denoted by a_1,a_2, and β_3 and $\mathbf{A}_i\,(i = 1, 2)$ are the Rivlin-Ericksen tensors that are defined in following relations:-

$$\mathbf{A}^1 = (\nabla \mathbf{U}) + (\nabla \mathbf{U})^T, \tag{6}$$

$$\mathbf{A}_n = \frac{\partial \mathbf{A}_{n-1}}{\partial t} + (\mathbf{U} \cdot \nabla)\mathbf{A}_{n-1} + \mathbf{A}_{n-1}(\nabla \mathbf{U}) + (\nabla \mathbf{U})^T \mathbf{A}_{n-1}; (n > 1) \tag{7}$$

By Darcy's law, we have

$$\mathbf{r}_1 = (\nabla \mathbf{p}) = -\frac{\phi}{\kappa}\mathbf{V}. \tag{8}$$

Here ϕ is the porosity, κ is the permeability of porous medium, $\mathbf{V}$ denotes apparent viscosity that varies from fluid to fluid. The apparent viscosity for unsteady unidirectional flow of a third grade fluid over a porous plate, is calculated as

$$\mathbf{V} = \mu + \alpha_1 \frac{\partial}{\partial t} - \alpha_1 W_0 \frac{\partial}{\partial y} + 2\beta_3 \left(\frac{\partial u_1}{\partial y}\right)^2, \tag{9}$$

using Eq. (9) in Eq. (8), over a porous plate the x-component of $\mathbf{r}_1$ for unidirectional flow is

$$r_x = -\frac{\phi}{\kappa}\left[\mu + \alpha_1 \frac{\partial}{\partial t} - \alpha_1 W_0 \frac{\partial}{\partial y} + 2\beta_3 \left(\frac{\partial u}{\partial y}\right)^2\right] u_1. \tag{10}$$

All the required calculated terms and incorporated in Eq. (3) we get the following governing equation in the absence of the modified pressure gradient i.e.

$$\begin{aligned}
\rho\left[\frac{\partial u_1}{\partial t} - W_0 \frac{\partial u_1}{\partial y}\right] &= \nabla \cdot \left[\mu \frac{\partial u_1}{\partial y} + \alpha_1 \left(\frac{\partial^2 u_1}{\partial y \partial t} - W_0 \frac{\partial^2 u_1}{\partial y^2}\right) + 2\beta_3 \left(\frac{\partial u_1}{\partial y}\right)^3\right] \\
&\quad - \frac{\phi}{\kappa}\left[\mu + \alpha_1 \frac{\partial}{\partial t} - \alpha_1 W_0 \frac{\partial}{\partial y} + 2\beta_3 \left(\frac{\partial u_1}{\partial y}\right)^2\right] u_1, \\
\rho\left[\frac{\partial u_1}{\partial t} - W_0 \frac{\partial u_1}{\partial y}\right] &= \mu \frac{\partial}{\partial y}\left(\frac{\partial u_1}{\partial y}\right) + \alpha_1 \frac{\partial}{\partial y}\left(\frac{\partial^2 u_1}{\partial y \partial t}\right) - \alpha_1 W_0 \frac{\partial}{\partial y}\left(\frac{\partial^2 u_1}{\partial y^2}\right) + 2\beta_3 \frac{\partial}{\partial y}\left(\frac{\partial u_1}{\partial y}\right)^3 \\
&\quad - \frac{\phi}{\kappa}\left[\mu u_1 + \alpha_1 \frac{\partial u_1}{\partial t} - \alpha_1 W_0 \frac{\partial u_1}{\partial y} + 2\beta_3 \left(\frac{\partial u_1}{\partial y}\right)^2 u_1\right], \\
\rho\left[\frac{\partial u_1}{\partial t} - W_0 \frac{\partial u_1}{\partial y}\right] &= \mu \frac{\partial^2 u_1}{\partial y^2} + \alpha_1 \frac{\partial^3 u_1}{\partial y^2 \partial t} - \alpha_1 W_0 \frac{\partial^3 u_1}{\partial y^3} + 6\beta_3 \left(\frac{\partial u_1}{\partial y}\right)^2 \frac{\partial^2 u_1}{\partial y^2} \\
&\quad - \frac{\phi}{\kappa}\left[\mu u_1 + \alpha_1 \frac{\partial u_1}{\partial t} - \alpha_1 W_0 \frac{\partial u_1}{\partial y} + 2\beta_3 \left(\frac{\partial u_1}{\partial y}\right)^2 u_1\right].
\end{aligned} \tag{11}$$

The exact and approximate solution of Eq. (1) is obtained by employing the following initial and boundary conditions

$$u_1(0,t) = u_0 V(t), t > 0,$$

$$u_1(y,t) \to 0 \quad as \quad y \to \infty, t > 0,$$

$$u_1(y,t) = g(y), y > 0.$$

Incorporating the following dimensionless quantities given as

$$\bar{u_1} = \frac{u_1}{u_0}, \bar{y} = \frac{u_0 y}{v}, \bar{t} = \frac{u_0^2}{v}, \bar{\alpha_1} = \frac{\alpha_1 u_0^2}{\rho v^2}$$

$$\bar{\beta_3} = \frac{2\beta_3 u_0^4}{\rho v^3}, \bar{\phi} = \frac{\phi v^2}{\kappa u_0^2}, \bar{W_0} = \frac{W_0}{u_0}.$$

Hence the non-dimensional form of Eq. (11) and corresponding initial and boundary conditions are given as,

$$\begin{aligned}
\left[\frac{\partial \bar{u_1}}{\partial \bar{t}} - \bar{W_0} \frac{\partial \bar{u_1}}{\partial \bar{y}}\right] &= \frac{\partial^2 \bar{u_1}}{\partial \bar{y}^2} + \bar{\alpha_1} \frac{\partial^3 \bar{u_1}}{\partial \bar{y}^2 \partial \bar{t}} - \bar{\alpha_1} \bar{W_0} \frac{\partial^3 \bar{u_1}}{\partial \bar{u_1}^3} + 3\bar{\beta_3} \left(\frac{\partial \bar{u_1}}{\partial \bar{y}}\right)^2 \frac{\partial^2 \bar{u_1}}{\partial \bar{y}^2} \\
&\quad - \bar{\phi}\left[\bar{u_1} + \bar{\alpha_1} \frac{\partial \bar{u_1}}{\partial \bar{t}} - \bar{\alpha_1} \bar{W_0} \frac{\partial \bar{u_1}}{\partial \bar{y}} + \bar{\beta_3} \bar{u_1} \left(\frac{\partial \bar{u_1}}{\partial \bar{y}}\right)^2\right], \\
u_1(0,t) &= V(t), t > 0,
\end{aligned} \tag{12}$$

$$u_1(y,t) \to 0 \quad as \quad y \to \infty, t > 0, \qquad (13)$$

$$u_1(y,0) = g(y), y > 0.$$

We ignore bars of non-dimensional quantities just for the simplicity. Again writing Eq. (12) as

$$\frac{\partial u_1}{\partial t} = \mu_* \frac{\partial^2 u_1}{\partial y^2} + \alpha_* \frac{\partial^3 u_1}{\partial y^2 \partial t} - \alpha_* W_0 \frac{\partial^3 u_1}{\partial y^3} + \beta_1 \left(\frac{\partial u_1}{\partial y}\right)^2 \frac{\partial^2 u_1}{\partial y^2} - \beta_2 u_1 \left(\frac{\partial u}{\partial y}\right)^2 + W_0 \frac{\partial u_1}{\partial y} - \phi_* u_1 . \qquad (14)$$

3. Traveling wave approximation and Dynamical systems theory

Traveling wave solutions are one of the exclusive type of group invariant solutions which are invariable under a linear combination of time and space translations symmetry generators. It can be seen that the Eq. (14) concede the Lie point symmetry generators. Hence we can devise the traveling wave solutions for the model equation. The solution (invariant) corresponding to the generator $Y = X_1 + cX_2$ which denotes the traveling wave solution with constant wave speed c. This solution under the operator Y is given by

$$u_1(y,t) = f(\eta), \qquad \text{where} \qquad \eta = y - ct. \qquad (15)$$

By changing the variables, the equation (reduced) for Eq. (14) is.

$$-c\frac{df}{d\eta} = \mu_* \frac{d^2 f}{d\eta^2} - c\alpha_* \frac{d^3 f}{d\eta^3} - \alpha_* W_0 \frac{d^3 f}{d\eta^3} + \beta_1 \left(\frac{df}{d\eta}\right)^2 \frac{d^2 f}{d\eta^2} - \beta_2 f(\eta) \left(\frac{df}{d\eta}\right)^2 + W_0 \frac{df}{d\eta} - \phi_* f(\eta) . \qquad (16)$$

It can be seen that Eq. (16) is nonlinear in nature and to obtain the exact or numerical solution is tedious. After applying the traveling wave approximation we then apply the theory of dynamical systems to study the qualitative behavior of the problem. This theory has been rarely adopted in the literature and only a few papers have addressed this issue. To proceed further in this regard we have converted the third order differential equation into the system of three first order differential equations

$$\begin{aligned} f(\eta) &= y_1, \\ \frac{df}{d\eta} &= y_2 = \dot{y}_1, \\ \frac{d^2 f}{d\eta^2} &= y_3 = \dot{y}_2, \\ \frac{d^3 f}{d\eta^3} &= \dot{y}_3 \end{aligned},$$

$$\dot{y}_3 = \frac{1}{\alpha_*(W_0 + c)} \left[\mu_* y_3 + \beta_1 y_2^2 y_3 - \beta_2 y_1 y_2^2 + (W_0 + c) y_2 - \phi_* y_1\right]. \qquad (17)$$

The next step is the calculation of stagnation points/equilibrium points. These points are in fact the spatial locations at which the system is at rest or in steady state. For this we will solve Eq. (17) simultaneously and obtain a single critical point i.e. (0,0,0). The Jacobian matrix **A** at critical Point (0,0,0), is calculated to check the stability of the problem.

$$\mathbf{A} = \begin{bmatrix} 0 & 1 & 0 \\ 0 & 0 & 1 \\ \frac{-\phi_*}{\alpha_*(W_0+c)} & \frac{1}{\alpha_*} & \frac{\mu_*}{\alpha_*(W_0+c)} \end{bmatrix}$$

The characteristic polynomial i.e. det(**A**-λ **I**) = 0 is computed for the evaluation of eigenvalues of the problem given in Eq. (17)

$$\begin{aligned} -\lambda[-\lambda(\frac{\mu_*}{\alpha_*(W_0+c)} - \lambda) - \frac{1}{\alpha_*}] - 1[\frac{\phi}{\alpha_*(W_0+c)}] &= 0 \\ \lambda[\lambda^2 - \frac{\mu_*}{\alpha_*(W_0+c)}\lambda - \frac{1}{\alpha_*}] - \frac{\phi_*}{\alpha_*(W_0+c)} &= 0, \\ -\lambda^3 + \frac{\mu_*}{\alpha_*(W_0+c)}\lambda^2 + \frac{1}{\alpha_*}\lambda - \frac{\phi_*}{\alpha_*(W_0+c)} &= 0. \end{aligned} \qquad (18)$$

Linear stability analysis is executed to study the behavior (qualitative) on the basis of which global behavior can be visualized. In addition, the qualitative nature is very conscious to the dependent parameters. Hence it is essential to determine the plausible range of the important parameters. We have studied three cases based upon these parameters to determine the topological

structure. We fix our parameters as $\mu_* = a_* = 0.5; \phi_* = 0.2$ and the following three cases will depicts the dynamics of the problem.

3.1. Case 1: $(W_0 + c) > 0$

For the specific values of the parameters involved, the spectrum of the matrix that corresponds to the equilibrium solution (0,0,0) is

Eigenvalue	$\lambda_1 = 1.6431$	$\lambda_2 = -1.2412$	$\lambda_3 = 0.0981$
Eigen vector	0.3017	-0.4511	-0.9952
	0.4957	0.5599	-0.0976
	0.8144	-0.6950	-0.0096

Table 1: $W_0 = c = 1$

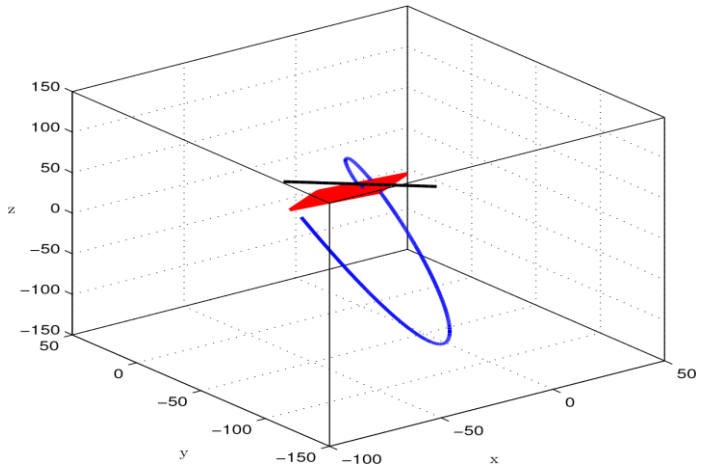

Figure 1: Eq.(17) is linearized about the stagnation point (0,0,0); pictorialization within the configurating box showing the plane of the unstable manifold and the line of the stable manifold.

Figure 1 represents the robust behavior of the linearized equation. The plane in the configurating box is the unstable manifold corresponding to the eigenvalues 1.6431 and
0.0981 whereas the line is the stable manifold representing the eigenvalue -1.2412.

3.2. Case 2: $(W_0 + c) < 0$

For the specific choice of the characterized parameters, the spectrum of the Jacobian matrix that corresponds to the equilibrium solution (0,0,0) is

Eigenvalue	$\lambda_1 = -1.6431$	$\lambda_2 = 1.2412$	$\lambda_3 = -0.0981$
Eigen vector	-0.3017	-0.4511	-0.9952
	0.4957	-0.5599	0.0976
	-0.8144	-0.6950	-0.0096

Table 2: $W_0 = c = -1$

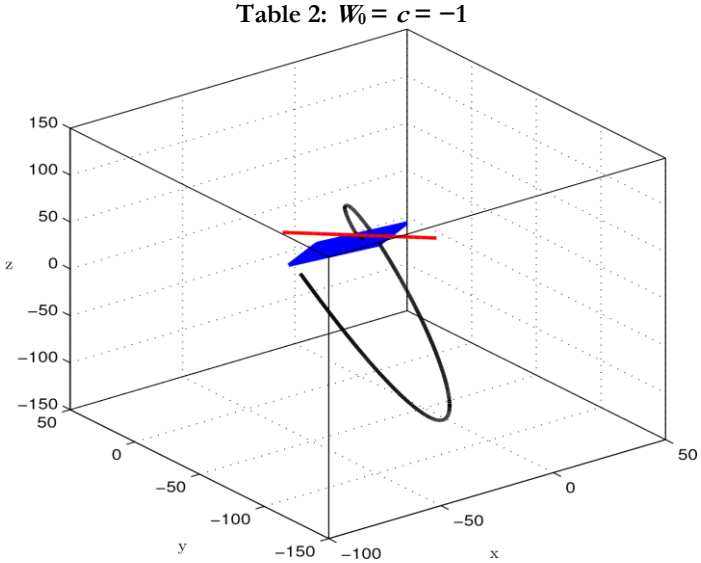

Figure 2: Eq.(17) is linearized about the stagnation point (0,0,0); pictorialization within the configurating box showing the plane of the stable manifold and the line of the unstable manifold.

Figure 2 shows the robustness of the linearized equation. The plane in the configurating box is the stable manifold corresponding to the eigenvalues -1.6431 and -0.0981 and the line drawn is the unstable representing the eigenvalue 1.2412. The trajectories starting in the stable manifold eventually dive into the direction of unstable manifold. Note that the flow of the original nonlinear equation drawn in the figure coincide the "nonlinear" only in the vicinity of the equilibria.

3.3. Case 3: $\phi_* = 1.6$

For the particular values of the parameters involved, the spectrum that corresponds to the critical point (0,0,0) is

Eigenvalue	$\lambda_1 = -1.5158$	$\lambda_2 = 1.0079 + 1.992i$	$\lambda_3 = 1.0079 - 0.1992i$
Eigen vector	-0.3415	0.5194-0.2137i	0.5194+0.2137i
	0.5176	0.5661-0.1119i	0.5661+0.1119i
	-0.7845	0.5929	0.5929

Table 3: $\phi_* = 1.6$

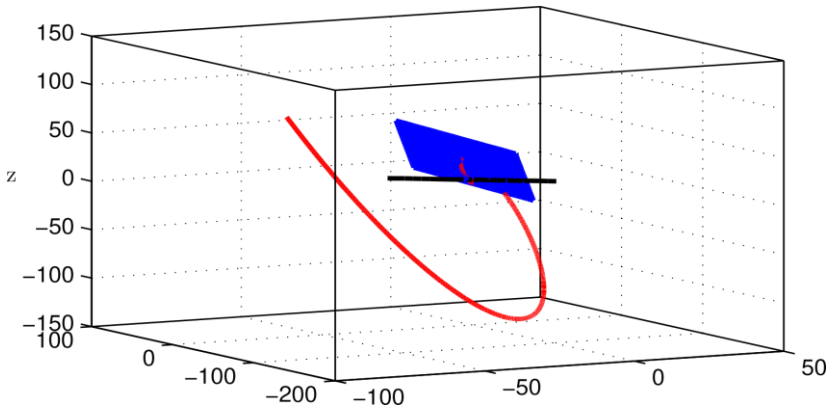

Figure 3: Eq.(17) is linearized about the stagnation point (0,0,0); pictorialization within the bounding box showing the plane of the unstable manifold.

Figure 3 represents the dynamics of the linearized equation. The plane in the configurating box is the unstable manifold corresponding to the eigenvalues 1.0079 + 0.1992*i* and
1.0079 − 0.1992*i*.

4. Stability Analysis using Normal Mode:

Stability analysis allows us to make an algebraic determination of critical point stability, which tells us how rapidly neighboring trajectories converge/diverge from the equilibrium points. Now we will study the behavior of third-order PDE.
Frrom Eq. 14, the general third-order PDE can be written as:

$$ut = \mu * uyy + a * uyyt - a * W0uyyy + \beta 1(uy)2uyy - \beta 2u(uy)2 + W0uy - \phi * u. \quad (19)$$

Linearized above Equation

$$\mu * uyy + a * uyyt - a * W0uyyy + W0uy - ut - \phi * u = 0. \quad (20)$$

Now, proposing the normal mode solution [24] of Eq. (20) and define:

$$u(y,t) = a(k)exp\left[iky + \lambda(k)t\right], \quad (21)$$

putting Eq. (21) in Eq. (20),

$$-\mu_* k^2 - \alpha_* k^2 \lambda(k) + i\alpha_* W_0 k^3 + iW_0 k - \lambda(k) - \phi_* = 0, \quad (22),$$

$$\begin{aligned}
\lambda(k)\left(\alpha_* k^2 + 1\right) &= -\mu_* k^2 - \phi_* + iW_0 k\left(\alpha_* k^2 + 1\right), \\
\lambda(k) &= \frac{-\left(\mu_* k^2 + \phi_*\right) + iW_0 k\left(\alpha_* k^2 + 1\right)}{\left(\alpha_* k^2 + 1\right)}, \\
\lambda(k) &= -\frac{\left(\mu_* k^2 + \phi_*\right)}{\left(\alpha_* k^2 + 1\right)} + iW_0 k, \\
\Omega &= lub \quad Re\left[\lambda(k)\right], \\
\Omega &= lub\left[-\frac{\left(\mu_* k^2 + \phi_*\right)}{\left(\alpha_* k^2 + 1\right)}\right], \qquad -\infty < k < +\infty \\
\Omega &= -\left(\frac{\mu_*}{\alpha_*}\right) \qquad \text{where}
\end{aligned}$$

Therefore $\Omega < 0$. As we know that when $\Omega < 0$ our equation is strictly stable. We can say that our Eq. (20) is strictly stable. Also, knowing that if linearized equation is stable then it's nonlinear equation is also stable.So our Eq. (19) which is nonlinear in nature is also stable.

5. Bifurcation Analysis

The dynamical system theory is a contemporary approach used to study the topological behavior of the problem by discerning the stability. The stability of the solution is equally important but it essential to pin down the validity of the solution as time goes to infinity. In addition, the qualitative behavior is very delicate to the characterizing parameters. Hence, it is essential to determine the plausible range of the important parameters which can be discussed by drawing the bifurcation diagrams with respect to the parameters involved. These diagrams will predict the qualitative behavior of the problem depending upon the various parameters in advance e.g. W_0 and ϕ_*.

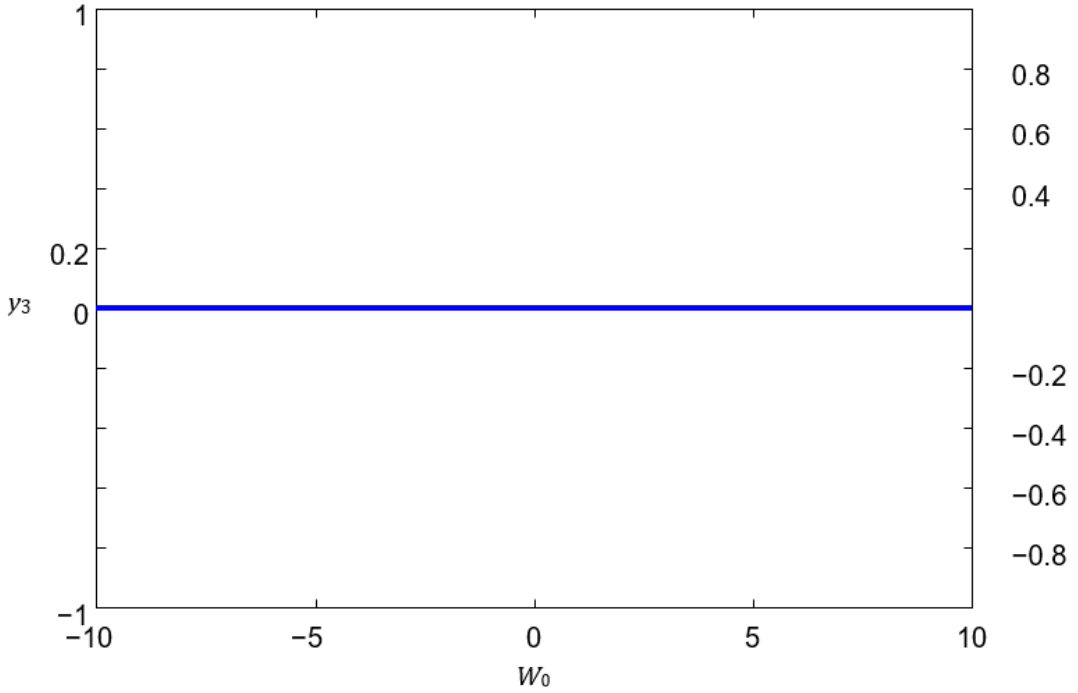

Figure 4: Bifurcation diagram plotted between W_0 and y_3. Here $W_0 + c > 0$

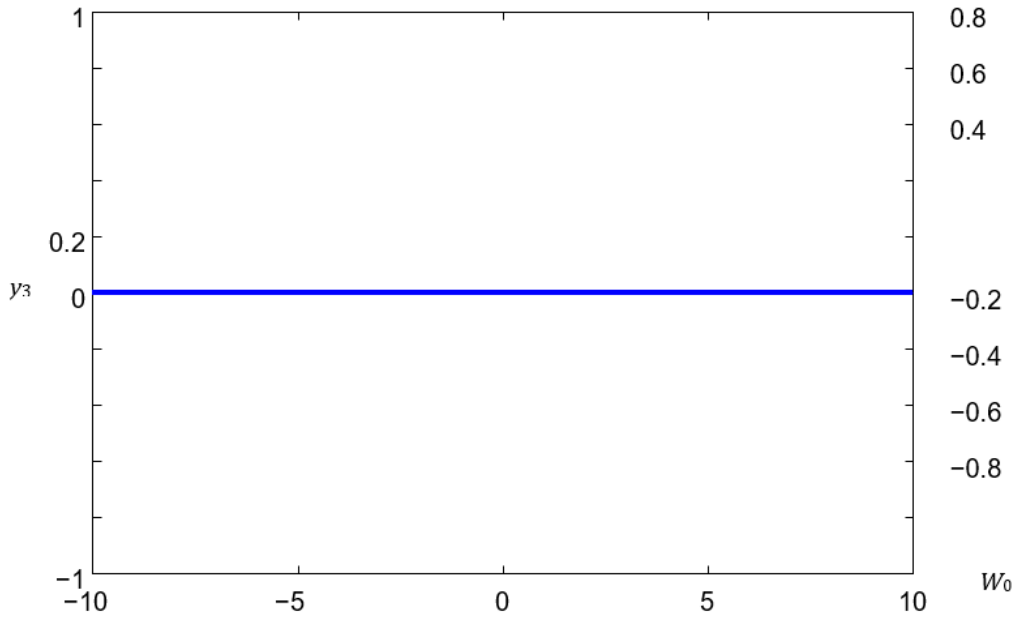

Figure 5: Bifurcation diagram plotted between W_0 and y_3. Here $W_0 + c < 0$

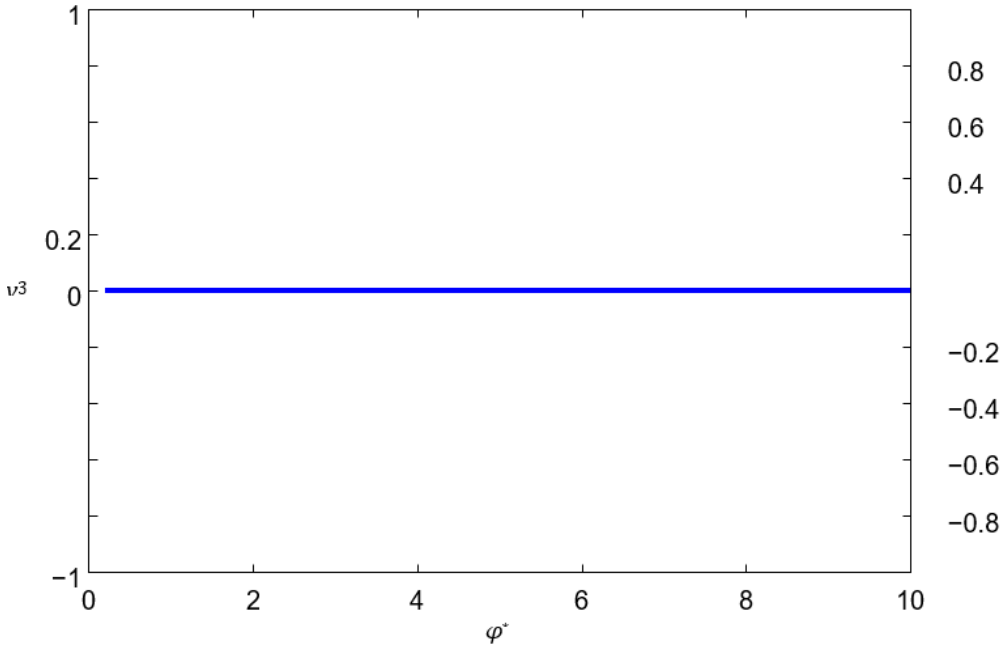

Figure 6: Bifurcation diagram plotted between ϕ_* and y_3

6. Numerical Schematic and Validation

The numerical solution of the nonlinear ordinary differential equation, given in Eq. (14) alongwith the boundary conditions specified in Eq. (13), is obtained using Finite Difference Method and Newton Raphson Method. We have used the central finite difference relations in the interior domain as well as the right boundary whereas forward finite difference relations are used at the left boundary, to dicretise the derivatives. The resulting system of equations are nonlinear which are then solved iteratively using the Newton's method. For the numerical scheme, the spatial domain is disretised using the step size $\Delta\eta = 10^{-2}$ and the Newton's method is iterated until the Euclidean norm between the consecutive solutions is less than 10^{-10}. The validation of the numerical solution is established the convergence of the solution subject to different initial conditions as discussed below.

$$c = 0.2, \mu = \alpha = 0.5, \phi = 0.2$$
$$\beta_1 = \beta_2 = 1, w_0 = 1$$

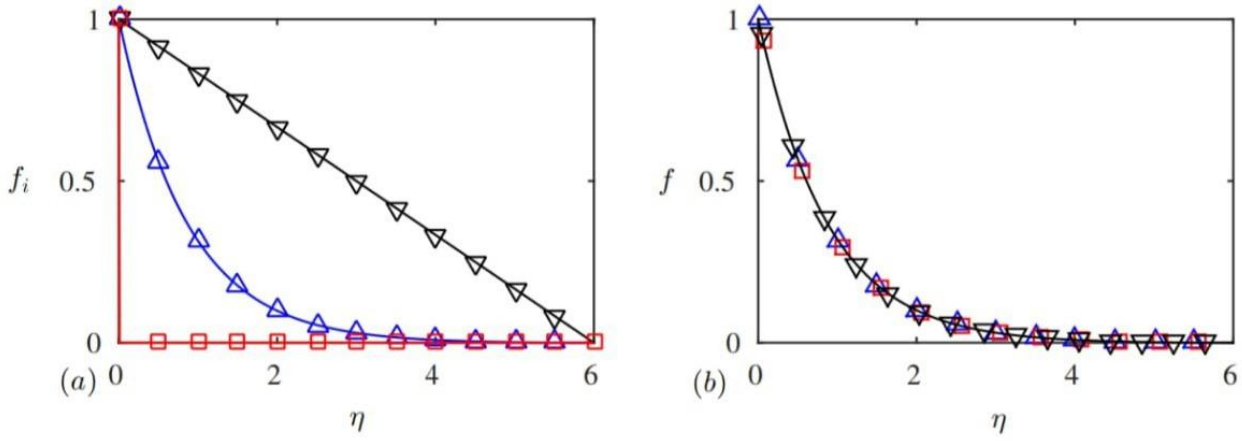

Figure 7: (a) The different initial conditions used in the iterative Newton's method, (b) shows the final solution that the Newton's method converges to with a tolerance of 10^{-10}. In (a), black line with downward triangles represents a linear curve satisfying the boundary conditions, blue line with upward triangles is the solution of the associated linear problem and red line with squares is the zero solution (in the interior domain).

The results presented in Figure 7 shows that the iterative Newton's method converges to the same solution for the three different initial conditions used in the test run. The curves in Figure 7(a) represented the various initial conditions used in our code. The black curve with downward triangles represent a simple linear curve satisfying the boundary condition. The blue curve with upward triangles is the (Finite Difference) numerical solution of the corresponding linear problem. As a particularly tough choice, due to presence of sharp gradients, we chose a step function which satisfies the boundary conditions and stays zero in the interior domain (shown in red with squares). For all three initial conditions, the interior procedure converges to the same solution which can be seen in Figure 7(b).

As an additional check, we compare our numerical solution with HAM solution of [6]

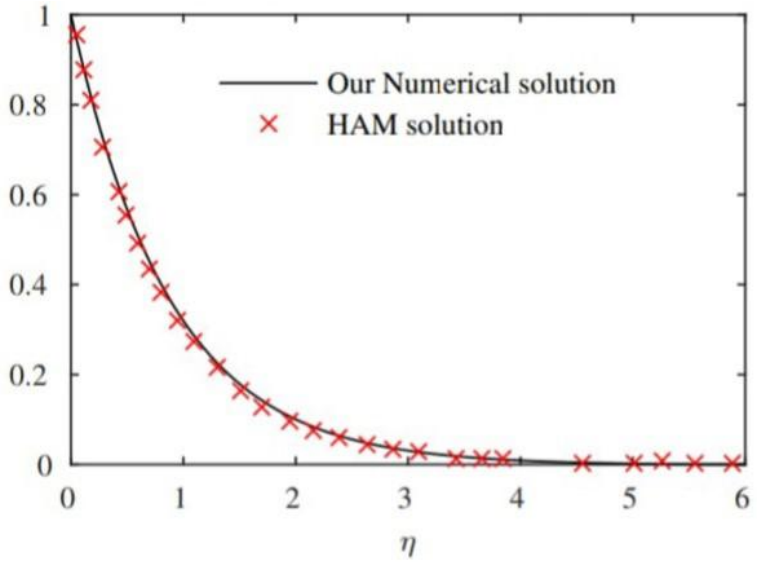

Figure 8: A comparison between our Numerical solution and the HAM solution given in [6]. The solid curve in black represents our numerical solution whereas red crosses are from the HAM solution of [6]. For this particular simulation, the flow parameters are set to $c = 0.2, \mu = \alpha = 0.5, \phi = 0.2, \beta_1 = \beta_2 = 1$ and $w_0 = 1$.

for $c = 0.2, \mu = a = 0.5, \phi = 0.2, \beta_1 = \beta_2 = 1$ and $w_0 = 1$. Figure 8, the solid curve shown in black represents our numerical solution whereas the red crosses are the (discrete) data points picks up from HAM solution of [6] for this particular case. It can be seen in the figure that the red crosses either overlap or reside in close proximity of the black curve showing an excellent agreement between our numerical solution and the HAM solution of [6]. The minor deviation of HAM results from our numerical results could possibly be due to the fact that the discrete points (red crosses) representing HAM solution are picked up from [6] using webplotdigitizer [17].

Figure 9 shows velocity profiles for different values of the suction parameter w_0. The result shown in solid black with upward triangles represent the solution for $w_0 = 0$ i.e.

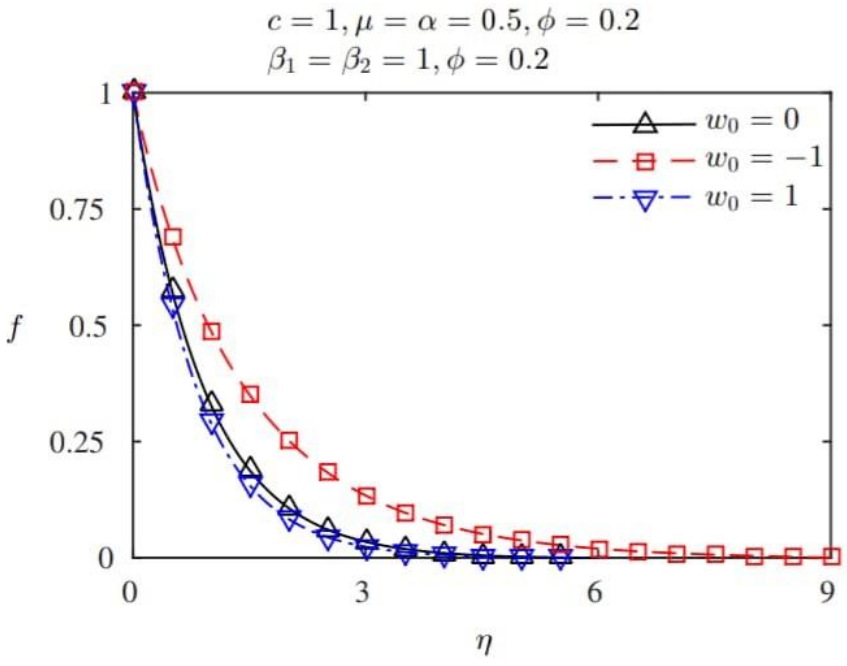

Figure 9: The velocity profiles, in terms of the similarity variable f, for the non-porous case ($w_0 = 0$, shown by solid black line with upward triangle markers), for injection ($w_0 = -1$, shown by dashed red line with square markers) and for suction ($w_0 = 1$, shown by dash-dotted blue line with downward triangle markers).

considering boundary to be non-porous. The dashed red curve with square markers shows the results corresponding to the injection case $w_0 = -1$ whereas the results for the suction ($w_0 = 1$) are given by dash-dotted blue curve with downward triangles. It should be noted that the physical problems, solved numerically, has an infinite domain but for numerical schemes it is necessary to consider a finite domain. As the physical effect diminishes far away from the source ($\eta = 0$), it is appropriate to

truncate the domain (for numerical convenience) at some suitable location far away from the source $\eta = 0$. For this particular reason, we had to consider a longer domain for the injection case to make sure that the domain is long enough to allow the accelerating effects being propagated from the source to dissipate. As for injection, the system receives an additional supply of momentum from the accelerated fluid steam being injected into the system due to which the velocities are propagated to larger distances compared to other cases (suction and non-porous). It is observed that the velocities for the injection case are larger than the non-porous case due to additional supply of momentum (energy) contributed by the fluid stream injected into the system. On the contrary, the velocities for the suction case are smaller than that of non-porous case due to the fact that the system experiences loss of energy due to the fluid escaping from the system.

7. Conclusion

The transitional symmetries are utilized for the reduction of the governing nonlinear PDEs equation of unsteady flow of an incompressible third-grade fluid, bounded by porous plate (infinite) which is moving in its plane with an arbitrary velocity. These nonlinear equations are reduced by traveling wave approximation and thereafter dynamical system theory is employed to study the qualitative behavior. Bifurcation diagrams and phase plots are plotted to predict the topological structure for the complete range of parameter values. With the help of boundary conditions, the numerical solution of the governing equation is found using the Finite Difference Method and the Newton-Raphson Method. The final solution is with a tolerance of 10^{-10} using the iterative Newton's method. We also checked our numerical solution against the HAM solution and found excellent agreement between both solutions.

References

[1] Akyildiz, F. T., Bellout, H., and Vajravelu, K. (2004). Exact solutions of nonlinear differential equations arising in third grade fluid flows. *International Journal of NonLinear Mechanics*, 39(10):1571–1578.

[2] Ali, N. and Ullah, K. (2019). Bifurcation analysis for peristaltic transport of a powerlaw fluid. *Zeitschrift fu¨r Naturforschung A*, 74(3):213–225.

[3] Ariel, P. D. (2003). Flow of a third grade fluid through a porous flat channel. *International Journal of Engineering Science*, 41(11):1267–1285.

[4] Asghar, Z. and Ali, N. (2014). Slip effects on streamline topologies and their bifurcations for peristaltic flows of a viscous fluid. *Chinese Physics B*, 23(6):064701.

[5] Asghar, Z. and Ali, N. (2015). Streamline topologies and their bifurcations for mixed convective peristaltic flow. *AIP Advances*, 5(9):097142.

[6] Aziz, T., Mahomed, F., Shahzad, A., and Ali, R. (2014). Travelling wave solutions for the unsteady flow of a third grade fluid induced due to impulsive motion of flat porous plate embedded in a porous medium. *Journal of Mechanics*, 30(5):527–535.

[7] Cortell, R. (2007). Mhd flow and mass transfer of an electrically conducting fluid of second grade in a porous medium over a stretching sheet with chemically reactive species. *Chemical Engineering and Processing: Process Intensification*, 46(8):721–728.

[8] Erdogan, M. E. and Imrak, C. E. (2005). On unsteady unidirectional flows of a second grade fluid. *International Journal of Non-Linear Mechanics*, 40(10):1238–1251.

[9] Fosdick, R. and Rajagopal, K. (1980). Thermodynamics and stability of fluids of third grade. *Proceedings of the Royal Society of London. A. Mathematical and Physical Sciences*, 369(1738):351–377.

[10] Hayat, T. and Kara, A. (2006). Couette flow of a third-grade fluid with variable magnetic field. *Mathematical and Computer Modelling*, 43(1-2):132–137.

[11] Hayat, T., Kara, A., and Momoniat, E. (2003). Exact flow of a third-grade fluid on a porous wall. *International Journal of Non-Linear Mechanics*, 38(10):1533–1537.

[12] Hayat, T., Mambili-Mamboundou, H., and Mahomed, F. (2008). Unsteady solutions in a third-grade fluid filling the porous space. *Mathematical Problems in Engineering*, 2008.

[13] Jim´enez-Lozano, J. and Sen, M. (2010). Streamline topologies of two-dimensional peristaltic flow and their bifurcations. *Chemical Engineering and Processing: Process Intensification*, 49(7):704–715.

[14] Makinde, O. D. (2009). Thermal criticality for a reactive gravity driven thin film flow of a third-grade fluid with adiabatic free surface down an inclined plane. *Applied Mathematics and Mechanics*, 30(3):373–380.

[15] Rajagopal, K., Szeri, A., and Troy, W. (1986). An existence theorem for the flow of a non-newtonian fluid past an infinite porous plate. *International Journal of Non-Linear Mechanics*, 21(4):279–289.

[16] Rivlin, R. S. and Ericksen, J. L. (1997). Stress-deformation relations for isotropic materials. *Collected Papers of RS Rivlin*, pages 911–1013.

[17] Rohatgi, A. (2014). Webplotdigitizer user manual version 3.4. *URL http://arohatgi. info/WebPlotDigitizer/app*, pages 1–18.

[18] Szeri, A. and Rajagopal, K. (1985). Flow of a non-newtonian fluid between heated parallel plates. *International Journal of Non-Linear Mechanics*, 20(2):91–101.

[19] Ullah, K. and Ali, N. (2019). Stability and bifurcation analysis of stagnation/equilibrium points for peristaltic transport in a curved channel. *Physics of Fluids*, 31(7):073103.

[20] Vajravelu, K. and Rollins, D. (2004). Hydromagnetic flow of a second grade fluid over a stretching sheet. *Applied Mathematics and Computation*, 148(3):783–791.

[21] Vieru, D., Siddique, I., Kamran, M., and Fetecau, C. (2008). Energetic balance for the flow of a second-grade fluid due to a plate subject to a shear stress. *Computers & Mathematics with Applications*, 56(4):1128–1137.

[22] Yasmeen, S., Asghar, S., Anjum, H. J., and Ehsan, T. (2019). Analysis of hartmann boundary layer peristaltic flow of jeffrey fluid: Quantitative and qualitative approaches. *Communications in Nonlinear Science and Numerical Simulation*, 76:51–65.

[23] Yu¨ru¨soy, M. and Pakdemirli, M. (2002). Approximate analytical solutions for the flow of a third-grade fluid in a pipe. *International Journal of Non-Linear Mechanics*, 37(2):187–195.

[24] Zauderer, E. (2011). *Partial differential equations of applied mathematics*. John Wiley & Sons.